Pulsed Magnetic Field Treatment of TiAlSiN Coated Milling Tools For Improved Cutting Performances

Hao Qu
Sichuan University
Lin Zhang
Sichuan University
Zhe Chen
Sichuan University
Lei Zhang
Sichuan University
Kyle Jiang
University of Birmingham
Jian Liu (liujian@scu.edu.cn)
Sichuan University

Research Article

Keywords: Pulsed magnetic treatment, Coated tool, Cutting force, Cutting vibration Residual stress, Adhesion strength

Posted Date: December 16th, 2021

DOI: https://doi.org/10.21203/rs.3.rs-1148443/v1

Version of Record: A version of this preprint was published at The International Journal of Advanced Manufacturing Technology on April 18th, 2022. See the published version at https://doi.org/10.1007/s00170-022-09145-9.

Abstract

In this study a pulsed magnetic treatment was attempted to improve the cutting performance of the TiAlSiN coated WC-12wt%Co cemented carbide end mills and the effects of the strength of the pulsed magnetic field on the cutting forces, the cutting vibrations, the tool wear, the machined surface roughness and mechanical properties were investigated. It is found that the cutting performances of the coated tools are successfully improved with a relatively lower cutting force and less wear area. The average resultant cutting force Fxy_{ave} decrease by 14.53% in the last machining process when the optimum processing parameters of 0.5T magnetic field is used, accompanying a maximum decrease of 46.8% in the cutting vibration. The maximum reductions of 57.65% and 25.4% in the flank wear and the average surface roughness of the workpiece are obtained respectively after the treatment. Both the hardness and toughness of the cemented carbides are slightly improved with the imposition of the field. The improvements in the cutting performance of the tool are attributed to the enhanced adhesion strength between the coating and matrix, which is caused by the increased compressive residual stress induced by the PMT.

1 Introduction

With the development trend of high-speed, high-precision, and high-efficiency cutting in the modern machining industry, cutting tools require increasingly exceptional cutting performances to maintain an excellent machining accuracy, a good surface finish, and a high-efficiency and low-cost production[1, 2]. Previously many studies were conducted to improve the cutting performance of cutting tools and they mainly focused on reducing tool wear, extending tool life and improving the surface quality of processed workpieces[3]. The commonly used method in the past was the heat treatment[4] and it usually took dozens of hours to improve the overall microstructure during the heat treatment, thereby improving the physical and mechanical properties of cutting tools to enhance their cutting life. Although the heat treatment process could treat samples on a large scale, it is usually time-consuming[5] and incurs a high cost. In recent years, as an emerging technology in manufacturing research, the pulsed magnetic treatment (PMT) receives enormous attention since it can modify the material to improve the microstructures and performances of the materials in a very short time[6]. Many investigations then used the PMT to treat cutting tools of different materials such as HHS[7], cemented carbide[5], ceramic metal[8], and super-hard materials[9] for enhanced cutting performances. The modification effects induced by the PMT on the cutting performance is usually associated with an increased surface hardness, a reduction in friction, an extended wear life, a delayed crack growth and an improved residual stress distribution[5]. Ma et al. [7] treated M42 HHS micro-cutting tools using the PMT and found that lattice distortion and the precipitation of a large number of dispersed carbides occurred in the tool material. Bataineh et al. [10] applied pulsed magnetic fields to HHS twist drills and demonstrated an increase in tool lifetime by as much as 35% in aggressive cutting conditions. Similar to the HHS tool, the introduction of the PMT renders the cemented carbide tool with an increasing dislocation density, which tended to strengthen the matrix and improve the cutting performance. Liu et al. [5]studied the effect of

PMT on the milling performance of cemented carbide end mills, and found that pulsed magnetic treatment tools could significantly reduce the milling force and reduce wear by 35% when milling a low-carbon steel. The significant improvement in the milling performance was attributed to the increase in the Vickers hardness and transverse rupture strength (TRS). Yuan et al. [11] studied the relation between the coupled fields and the cutting performance of the cemented carbide tool and it is believed that residual stress, magnetostriction effect and the field-induced defects were closely associated with the tool life. Besides the cutting tools, the PMT is found to be effective in the modification of other materials. Fahmi et al reported an increased fatigue life of low carbon steels for cyclic loading after the treatment. Cai et al. [12]showed that the pulsed magnetic field could reduce the residual stress of Cr4Mo4V steel and Yip et al. [9] found that the Super-hard diamond tools treated by pulsed magnetic field could reduce the adhesive wear and improve the machined surfaces of titanium alloy.

Previous literatures indicate that the PMT can improve the microstructures and performances of the cutting tools. However, to the best knowledge of the author, there are scarce investigations on the treatment of the coated tool using the pulsed field. Therefore, in the presented study the PMT was introduced to treat the TiAlSiN coated WC-12wt%Co cemented carbide end mills to evaluate the effects of the pulsed field on the cutting performance of the tool. The results obtained are expected to provide insights for the potential applications of this post-treatment in the industry of coated tools.

2 Experimental Procedures

2.1 Cutting tool and workpiece material

Milling experiments were performed using commercially replaceable TiAlSiN coated end mills of WC-12wt%Co cemented carbides (Dongguan FULLANTI Tools Co., Ltd, China). The tool geometry and the key properties of deposited TiAlSiN layer are summarized in Table 1. The workpiece employed in the milling experiment is AISI 316L stainless steel with a size of 20×10×3cm^3 and the mechanical properties of AISI 316L stainless steel are shown in the Table 2. To evaluate the interface properties between the coating and the matrix, a TiAlSiN coating is deposited on cemented carbide substrate by Physical Vapor Deposition (PVD) technique.

Table 1
Geometrical and properties of the TiAlSiN coated tool

Parameters	Values
Tool diameter (mm)	4
Overall length (mm)	50
Milling flute number	4
Helix angle, β (°)	35
Coating thickness (μm)	1.5
Coating hardness (HV)	3500
Friction coefficient (VSNI)	0.45
Oxidation resistance temperature (℃)	950
Thermal conductivity (W/m·K)	0.6~0.7
Processing application	Stainless steel, Titanium alloy

Table 2
Mechanical performances of AISI 316L stainless steel

Properties	Value
Hardness (HV)	195 ± 5
Elastic modulus (Gpa)	200
Density (g/cm^3)	7.98
Poisson's ratio	0.30
Thermal conductivity (W/m·K)	16.2

2.2 Pulsed magnetic field treatment

A schematic diagram of magnetic field treatment process with a 0.5 field intensity is given in Figure 1 and the direction of pulsed magnetic field is perpendicular to that of the milling tool. The pulsed magnetic field with a specific waveform was introduced by adjusting the coil current and the TiAlSiN coated cemented carbide end milling tools (WC-12wt%Co) were magnetized 20 times with intensities from 0.5T to 1.5T with a pulse interval of 10 s.

2.3 Milling experiments

The milling experiments were conducted on AISI 316L stainless steels using a TEMA VL1060A CNC vertical machining center and the milling parameters are compiled in Table 3. A typical linear cycle cutting method was employed in this study and the distance of each feeding was 100 mm. After each

cutting was completed, the tool returned to the starting point, and this feeding process was repeated 20 times along the axial direction until the axial cutting depth reached 6mm.

Table 3
Milling parameters

Parameters	Values
Spindle speed, n (r/min)	5500
Cutting speed, v_c(m/min)	69
Feed rate, v_r (mm/tooth)	0.27
Axial depth of cut, a_p (mm)	0.30
Radial depth of cut, a_e (mm)	2.00
Cutting fluid	Water-based emulsion

2.4 Measurement and processing of the cutting force signal

A Kistler 9257B three-way dynamometer with a Kistler 5019A multi-channel charge amplifier was installed on the AISI 316Lstainless steel workpiece through four bolts and was used to obtain the cutting force component values in three direction (F_x、F_y、F_z) during the cutting process at a sampling frequency of 5 kHz. Figure 2shows the experimental step and note that the axial cutting depth (a_p=$0.3mm$) is less than the radial cutting depth ($a_e = 2.0mm$) and the tool diameter ($D = 4.0mm$), therefore, the axial cutting force F_z is much smaller than the horizontal component force (the feed force F_x、the cross-feed force F_y), and can be considered as negligible in this study. The resultant cutting force F_{xy} and Fxy_{ave} can calculated by the Eq. 1 (N is the number of cutting force data points).

$$Fxy_i^2 = Fx_i^2 + Fy_i^2 (i = 1 \ldots N),\ Fxy_{ave} = \frac{1}{N}\sum_{i=1}^{N} F_{xy_i}$$

1

Milling is a typical multi-edge intermittent cutting process. During the cutting process, the periodic changes of cutting force and chip thickness will produce the cutting vibrations, which can be manifested and reflected by the fluctuation of the cutting force component during the machining process[13]. In the experiment, the signal characteristic value (feature energy) was extracted to reflect the tool wear, as suggested by the report[8]. In the present work the discrete horizontal cutting force signals were decomposed over j =3 levels using Daubechies 5 wavelets, which produced 2^3 different sets of coefficients χ_m^j(t) for a data vector with n data points, where m = 1, 2, …,2^3, and the length of χ_m^j(t) is $n/2^j$. According to the wavelet packet coefficients of different sets, the signal in the frequency interval [f_s

(m-1)/$2^j f_s$m/2^j] can be reconstructed as p_m^j(t), wheref_s is the sampling frequency. The feature energy of the mth signal band can be calculated by Eq. 2.

$$E_{j,m} = \int \left|S_{j,m}(t)\right|^2 dt = \sum_{k=1}^{n} \left|x_{m,k}\right|^2$$

2

where $x_{m,k}$ is the amplitudes of the discrete points of the reconstruction signal $S_{j,m}$(m= 1, 2,.., 2^3; k = 1, 2,...,n; n is the number of discrete sampling points of the signal).

2.5 Characterization

After milling experiments, a scanning electron microscope (SEM) equipped with an energy dispersion spectrometry (EDS) was used to analyze the final morphology and elemental distribution of the flank worn surface of the TiAlSiN coated milling tools. The surface topography of the workpiece and surface roughness (Ra) values along the feed direction was measured by a BRUKER Contour GT-K, and the residual stress developed in the TiAlSiN coating was characterized by X-ray residual stress analysis equipment (Japan Pulstec's model μ-X360). The adhesion strength between the TiAlSiN coating and the cemented carbide substrate was tested by Rockwell indentation with a load of 60kg, and the indentation morphology was observed by a optical microscope (OM). Furthermore, a scratch tester (MFT-4000) was employed to quantitatively analyze the adhesion strength between the TiAlSiN coating and the WC-12%wtCo cemented carbide substrate under applied a load from 0 up to 150 N with a loading speed of 100 N/min. The scratch tracks were examined by an OM to identify the coating failure morphologies. Scratch tracks were examined by a SEM to identify the coating failure morphologies and the critical load was confirmed by both the scratch tracks. Vickers hardness and indentation fracture toughness values were obtained using a Vickers hardness tester on WC-12wt%Co cemented carbide samples with the size of $20 \times 5 \times 5mm^3$. At least five indentation points are tested for the reliable result.

3. Results And Discussions

3.1 Cutting forces

Cutting force is an indicator of the state of tool wear during machining and Figure 3 shows the average cutting force Fx_{ave}、Fy_{ave} and Fxy_{ave} during the steady-state cutting for the untreated and treated samples. It can be seen that there is hardly appreciable change in the cutting force of Fx_{ave} for all samples with the increasing cutting length due to a very short period in the X direction. Contrary to the Fx_{ave}, the cross-feed cutting force Fy_{ave} for all tools increases progressively with the increase of the cutting distances (Figure 3.b) and the cutting force for the untreated sample increases more sharply than that for treated samples. In addition, 0.5T treated sample exhibit the slowest increases in the cutting force. It is widely known that tool wear increases with increasing cutting distances, and the tool cutting edges become blunted and lose their original geometries gradually. The deterioration of the tool geometry

leads to an increase in the cutting force [14] and therefore, it is expected that the wear area for the untreated sample will be significantly higher than that for the treated samples. The variation of the resultant cutting force Fxy_{ave} with the cutting distance shown in Figure 3.c is almost the same as that of the Fy_{ave}(Figure 3.b). This is mainly due to the fact that the cutting period in the Y direction is much longer than that in the X direction and the feed in the Y direction during the cutting process is much larger than that in the X direction. As a result, the F_y is much greater than F_x during the cutting period. Similar to what observed in Fy_{ave}, the tool treated with a 0.5T field presents the lowest value in the resultant cutting force and the values of Fxy_{ave} for the 0.5T and 1.0T treated tools are 14.53% and 3.61% lower than the value of Fxy_{ave} for the untreated tool respectively in the last feed.

3.2 Cutting vibrations

As the tool wears, the cutting process becomes unstable and the cutting vibration increases. Based on the wavelet packet decomposition (WPD), the main cutting force $F_y$during the last feed was decomposed and reconstructed in the time-frequency domain, and the static cutting force characteristics and dynamic cutting vibration characteristics related to tool wear characteristics were extracted through high and low frequency separation. In addition, the wavelet packet coefficient energy value (feature energy) of the $\mathrm{m\text{-}th}$ signal band calculated according to Eq. (1-2) and the total feature energy for all tools during the last feed were used as the indicator of tool wear and cutting stability as illustrated in Figure 4. It can be seen that for all tools, the feature energy in the E1 and E2 bands accounts for more than 95% of the total feature energy and the feature energy is mainly distributed in the first frequency band (E1).

The reconstructed signal in E1 band implies the static cutting forces and the reconstructed signal in the high frequency band (E2) suggests the dynamic cutting vibrations caused by periodic cutting during milling process. The feature energies in the E1 band for all treated tools are lower than the feature energy for the untreated tool. In addition, tools treated by 0.5T and 1.0T fields exhibit significant lower energies compared to the untread tool. These differences in feature energies of the static cutting forces correspond exactly to the variation of the cross-feed cutting force Fy_{ave} in Figure 3.c. Comparing the feature energy of the second frequency band (E2), it can be found that the degree of the dynamic cutting vibrations has decreased after PMT and in particular, the cutting vibration energy for the tool treated by a 1.0T field is the lowest, which is 46.8% lower than that of the untreated tool. For the total feature energy, since the feature energy of the static cutting forces is much greater than that of the dynamic cutting vibrations, the tool treated by the 0.5T field still has the lowest energy, and is decreased by 27.09% as compare to the untreated tool during the last feed. These results indicate the PMT provides a more stable cutting process at a lower vibrational energy, as reported previously by Yuan et al [11].

3.3 Tool wear

Asan important indicator of the milling performance of the tool[15], flank wear is examined and their morphologies are shown in Figure 5.As each end mill is comprised of two long cutting edges and two short cutting edges, typical failure modes of the cutting edge are provided for the analysis. It can be seen from the Figure 5 that nose wear (thenormal flank wear), build-up edge (BUE), chipping and fracture of the

cutting edge are noted after the cutting process. In the case of untreated tools (Figure 5.a1), it can be observed obviously that there is a large area of coating delamination and flaking occurred on the flank face and the severe unevenness of the coating along the cutting edge may in turn initiate ploughing instead of shearing during the cutting and led to the catastrophic tool fracture, as shown in Figure 5.b1. It is expected thatthe poor cutting edge integrity and non-uniform of the coating along the cutting edge lead to greater ploughing forces, inturn, cause immediatecatastrophic fracture of the tool[16]. In the sharp contrast, the tool treated by the 0.5T field exhibits the significantly smaller wear area of the coating and slight chipping wear, which suggests that a significant portion of TiAlSiN coating still retains on the end mill surface. As tribo-oxidation behavior causes the TiAlSiN coating to form an alumina surface protective layer with high chemical and thermodynamic stability, which critically helps prevent the stainless steel from sticking to the tool, coatings remaining on the flank face will reduce the amount of the BUE formed during the cutting process. The increase in the strength of the field treatment to1T and 1.5 T leads to increasing flaking area of the coating and the occurrence of the chipping. However, compared with the untreated tool, the chipping area of the cutting edge of the tool treated by 1.0T and 1.5T field is reduced. In general, the untreated tool presents severe tool wear and the significant distortion of cutting edge shapes weaken the strength of the cutting edge, resulting in deteriorated cutting performance and inferior service life [17]. In contrast, the treated tools exhibit relatively less wear and maintain a better cutting edge integrity. It can be inferred that the degree of wear of tools field is reduced after the PMT and consistent with the result of the cutting force (Figure 3). What should be noted is that the relative movement between the workpiece and the tool promotes the cyclic removal of BUE, and the formation and tearing off of the BUE during cutting usually lead to the coating delamination or flaking, and the machining forces instability, which results in cutting edge chipping [18, 19], as evident in Figure 5.a1. Moreover, the cyclic formation and disappearance of the BUE caused by its periodic fractures will further leads to the cutting instability, which causes the cutting vibration and different tool wear [20].

VB_{max} and $\overline{VB_{max}}$ values of four cutting edges for each tool were compiled in Figure 6 based on SEM images to further evaluate the cutting performance of tools. According to ISO standard, the flank wear value of 0.3mm is used as the standard of tool wear failure. Note that the differences of the VB_{max} values for the same tool are very large as four cutting edges in the end mill possess varying lengths. It can be seen that the $\bar{VB}_{max}$ values of tools treated by pulsed magnetic field decrease dramatically in comparison with the that of untreated tool. In particular, the shape of most cutting edges for the tool treated by the 0.5T field remains relatively intact and present the smallest wear area, which results in a 57.65% decrease in the $\bar{VB}_{max}$.

3.4 Surface roughness

Surface roughness is one of the most important factors affecting the appearance of the product, reliability and functionality[21]. The average surface roughness (ASR, Ra) is a common measure for evaluating the surface texture and the three-dimensional surface morphology and average surface roughness of the workpiece are shown in Figure 7.It can be observed that the surface exhibits a typical

milling surface morphology with a semicircular ridge formed by the circular motion of the cutting edge in the feed direction. The treated tools all show a relatively smoother surface morphology and smaller surface roughness. As indicated previously, the loss ofthe flank edges (catastrophic cutting edge fracture) under dynamic vibrations tends to cause higher radial roughness (Ra) values and lead to more noticeablefeed mark embossments[22]. Therefore, the better workpiece surface finish is attributed to the better preservation of the sharpness of the cutting edge. In particular, surface morphology produced by the 0.5T treated tool shows the smoothest surface and compared with the untreated tool, the average surface roughness of the tool treated by the 0.5T field is reduced by 25.4%. As the smaller profile height between surface peaks and valley can translate into a smoother and stronger machined surface with better dimensions and mechanical properties[22], the difference in the surface roughness is attributed to the fact that a less wear tool with a better integrity of the cutting edge tends to introduce a smaller ploughing effect and a better surface quality.

3.5 Residual stress

The above results indicate that 0.5 T field is the optimum processing parameter for improving the cutting performance of the coated tool. Therefore, the parameter was adopted for further comparison analysis. In most applications, a key factor in the service life and performance of coated components is the adhesion of the coating to the substrate. The premise of the protective function of surface coatings on cutting tools is that the coating has a good adhesion strength to the tool substrate during the service process [23]. The above results clearly indicate PMT can indeed improve the cutting performance of the coated tools and the improvement in the performance is closely associated with the adhesion strength of the TiAlSiN coating to the substrate.

The indentation test is employed to preliminarily evaluate the adhesion strength of the interface between the TiAlSiN coating and the cemented carbide substrate and the result is provided in Figure 8. It can be seen that a large area of the coating spallation around the indent is observed for the untreated sample, in addition to several large and long cracks and many short cracks. In comparison, the degree of the coating spallation and the formation of cracks are greatly reduced after the PMT, implying a better adhesion strength of the coating to the substrate induced by the pulsed field. For further analysis, the scratch experiment is employed to quantitatively analyze the adhesion strength (bonding force) and the scratch morphologies are shown in Figure 9. At the beginning of the scratch, the load is very low and the scratch is smooth due to the defects such as droplets and pits on the coating surface. As the load increases, transverse cracks begin to occur at the edges of the coating. Lc2 in Figure 9 represents the load value where the coating is continuous cracking along the scratch track which shows the real adhesion [24]. For the WC-12wt%Co sample deposited with TiAlSiN coating, a value of Lc2 equal to 83.24 N, is obtained before the treatment (Figure 9.a)

Whereas, Lc2 achieves the value of 92.02N (Figure 9.b) after PMT, which indicates a 10.55% increase in the bonding force and enhanced adhesion between the coating and this substrate with the introduction of the pulsed field. According to the previous literature [25], the residual stress developed in the coating structure is an important factor affecting the adhesion between a coating and a substrate. In addition,

since the compressive stress counteracts the crack initiation and propagation in the coating, they are considered as advantageous for loaded tools, and a higher compressive stress implies a longer service life of coated tools[26].The residual stress developed in the TiAlSiN coating of the tools are examined and the results are provided in Figure 10.It can be clearly seen that the residual stress developed in the TiAlSiN coating of the untreated sample is a compressive residual stress with a magnitude of 421Mpa; after PMT (0.5T), the compressive residual stress increases to 679Mpa, representing a remarkable 61% improvement. The increase in the residual compressive stress is expected to enhance the bonding strength between the TiAlSiN coating and the cemented carbide substrate, which is consistent with the adhesion strength result in Figure 9. Due to the enhancement of the adhesion strength after PMT, more TiAlSiN coating remains on the cutting edge to participate in subsequent cutting with less substrate exposure, which will be beneficial for the reduction of friction and thermal energy dissipation at the cutting zone. It is obvious that the reductions of cutting force and cutting heat effectively slow down the accumulation of deformation and internal damage in the cemented carbide substrate. As mentioned before, a higher temperature and a higher cutting force are the main reasons that cause the adhesion of work piece material onto the tool flank face and thus accelerating the tool wear. This enhancement of the adhesion strength will indirectly lead to the alleviation of BUE formation and shedding, which can avoid further damage to the non-shedding coating and the aggravation of the cutting vibrations. These factors (lower BUE formation and lower progressive build-up), coupled with the alleviation of the internal damage in the cemented carbide substrate while cutting, lead to the reduction of the probability of tool edge chipping and fracture, which can cause a lower ploughing force and a relatively small cutting vibration. Therefore, the enhancement of the adhesion strength of the TiAlSiN coating after PMT reduces the formation of BUE and the cutting vibrations, and chipping and fracture of the cutting edge are less prone to occur, resulting in a longer tool life and a better cutting performance.

3.6 Mechanical properties of the cemented carbides substrate

The Vickers hardness and fracture toughness of the cemented carbides matrix before and after the PMT are compiled in Figure 11 to assess mechanical properties of the substrate material. It can be seen in the Figure that the Vickers hardness of the carbide cemented material exhibits a marginal increase after PMT, while the indentation fracture toughness is increased substantially by 8% with the imposition of a pulsed magnetic field. Previous reports indicates that one of the major underlying mechanisms is such that the introduction of the pulsed magnetic field tends to promote the formation of the dislocations within the cemented carbides to strengthen the material. As a result, hardness of the materials presents a slight increase. Fracture toughness is a characterization of the ability of a material to prevent crack propagation. When a crack is formed, it tends to propagate along a path with the least resistance and usually presents a fast progress rate within the brittle materials. As the pulsed field strengthens the cemented carbides matrix, it is expected that the resistance to the crack path is enhanced, which reduces the crack growth rate. Accordingly, not only can the pulsed field alter the interface residual stress, but also can strengthen the substrate material to improve the toughness while maintaining the hardness. As a result, chipping and fracture of the cutting edge are less prone to occur after the PMT treatment.

4. Conclusion

This work used a pulsed magnetic field treatment to enhance the service life and cutting performance of the TiAlSiN coated WC-12wt%Co cemented carbide tool and the improved performances were evaluated by cutting forces, the cutting vibrations, the tool wear, and the machined surface roughness of the workpiece. The obtained results indicate that 0.5T field is the optimum processing parameter, under which the average resultant cutting force Fxy_{ave} decreases by 14.53% in the last machining process. An reduction of 57.65% in the flank wear $\overline{VB}_{max}$ is obtained after the PMT, with a reduction of 46.8% in the cutting vibration. The better cutting edge integrity of field treated tool weakens the ploughing effect on the surface of the workpiece, thereby obtaining a better surface finish of the workpiece. The compressive residual stress developed in the interface between the TiAlSiN coating and the cemented carbides substrate is considered the main reason to enhance the cutting performance.

These obtained results demonstrate that the proposed PMT is an effective and fast way to improve the lifetime and cutting performance of the coated tool, and can be beneficial to the future industrial application of the low strength, easy-to-produce and controllable magnetic fields.

Declarations

Ethics declarations

Funding

This work was supported by the National Nature Science Foundation of China (No. 51975390)

Competing interests

The authors declare no competing interests.

Data availability

Not applicable.

Code availability

Not applicable.

Ethics Approval

The authors declare that this manuscript was not submitted to more than one journal for simultaneous consideration. Also, the submitted work was original and has not been published elsewhere in any form or language.

Consent to participate/consent for publication

The authors declare that they participated in this paper willingly, and the authors declare to consent to the publication of this paper.

Author Contributions

Hao Qu: Methodology; Data curation; Writing - original draft

Lin Zhang: Formal analysis

Lin Zhang, Zhe Chen: Investigation

Lei Zhang: Validation

Kyle Jiang: Guidance and discussion

Jian Liu: Conceptualization; Funding acquisition; Project administration; Writing - review & editing

References

1. M. Wang, J. Wang, CHMM for tool condition monitoring and remaining useful life prediction, The International Journal of Advanced Manufacturing Technology, 59 (2011) 463-471.
2. J. Liu, S.-S. Zhu, X. Deng, J.-Y. Liu, Z.-P. Wang, Z. Qu, Cutting Performance and Wear Behavior of AlTiN- and TiAlSiN-Coated Carbide Tools During Dry Milling of Ti–6Al–4V, Acta Metallurgica Sinica (English Letters), 33 (2020) 459-470.
3. X. Liao, G. Zhou, Z. Zhang, J. Lu, J. Ma, Tool wear state recognition based on GWO–SVM with feature selection of genetic algorithm, The International Journal of Advanced Manufacturing Technology, 104 (2019) 1051-1063.
4. N.A. Özbek, A. Çiçek, M. Gülesin, O. Özbek, Investigation of the effects of cryogenic treatment applied at different holding times to cemented carbide inserts on tool wear, International Journal of Machine Tools and Manufacture, 86 (2014) 34-43.
5. J. Liu, C. Wei, G. Yang, L. Wang, L. Wang, X. Wu, K. Jiang, Y. Yang, A Novel Combined Electromagnetic Treatment on Cemented Carbides for Improved Milling and Mechanical Performances, Metallurgical and Materials Transactions A, 49 (2018) 4798-4808.
6. Y. Yang, Y. Yang, C. Liao, G. Yang, Y. Qin, Q. Li, M. Wu, Enhancing tribological performance of cemented carbide (WC-12Co) by pulsed magnetic field treatment and magnetofluid, Tribology International, 161 (2021) 107086.
7. L. Ma, X. Wang, Z. Liang, Y. Liu, D. Zhang, Machining mechanism in pulsed magnetic treatment for micro-tools, The International Journal of Advanced Manufacturing Technology, 101 (2018) 2391-2406.
8. M. Yuan, J. Wang, L. Wang, F. Zhong, K. Huang, Y. Tian, Electromagnetic coupling field strengthening of WC-TiC-Co cermet tools, Ceramics International, 47 (2021) 3747-3759.

9. W.S. Yip, S. To, Tool life enhancement in dry diamond turning of titanium alloys using an eddy current damping and a magnetic field for sustainable manufacturing, Journal of Cleaner Production, 168 (2017) 929-939.
10. O. Bataineh, B. Klamecki, B.G. Koepke, Effect of pulsed magnetic treatment on drill wear, Journal of Materials Processing Technology, 134 (2003) 190-196.
11. M. Yuan, J. Wang, M. Wang, K. Huang, L. Wang, Y. Tian, Enhanced carbide tool life by the electromagnetic coupling field for sustainable manufacturing, The International Journal of Advanced Manufacturing Technology, 108 (2020) 3905-3914.
12. z. Cai, X. Huang, Residual stress reduction by combined treatment of pulsed magnetic field and pulsed current, Materials Science and Engineering: A, 528 (2011) 6287-6292.
13. N.A. Kasim, M.Z. Nuawi, J. A. Ghani, M. Rizal, M.A.F. Ahmad, C.H. Che Haron, Cutting tool wear progression index via signal element variance, Journal of Mechanical Engineering and Sciences, 13 (2019) 4596-4612.
14. K. Aslantas, H.E. Hopa, M. Percin, İ. Ucun, A. Çicek, Cutting performance of nano-crystalline diamond (NCD) coating in micro-milling of Ti6Al4V alloy, Precision Engineering, 45 (2016) 55-66.
15. Y. Isik, Investigating the machinability of tool steels in turning operations, Materials & Design, 28 (2007) 1417-1424.
16. S.A. Khan, S. Shamail, S. Anwar, A. Hussain, S. Ahmad, M. Saleh, Wear performance of surface treated drills in high speed drilling of AISI 304 stainless steel, Journal of Manufacturing Processes, 58 (2020) 223-235.
17. P. Baowan, C. Saikaew, A. Wisitsoraat, Influence of helix angle on tool performances of TiAlN- and DLC-coated carbide end mills for dry side milling of stainless steel, The International Journal of Advanced Manufacturing Technology, 90 (2016) 3085-3097.
18. M.S.I. Chowdhury, B. Bose, G. Fox-Rabinovich, S.C. Veldhuis, Investigation of the Wear Performance of TiB2 Coated Cutting Tools during the Machining of Ti6Al4V Alloy, Materials (Basel), 14 (2021).
19. J.L. Endrino, G.S. Fox-Rabinovich, C. Gey, Hard AlTiN, AlCrN PVD coatings for machining of austenitic stainless steel, Surface and Coatings Technology, 200 (2006) 6840-6845.
20. N. Fang, P.S. Pai, S. Mosquea, The effect of built-up edge on the cutting vibrations in machining 2024-T351 aluminum alloy, The International Journal of Advanced Manufacturing Technology, 49 (2009) 63-71.
21. P. Haja Syeddu Masooth, V. Jayakumar, G. Bharathiraja, Experimental investigation on surface roughness in CNC end milling process by uncoated and TiAlN coated carbide end mill under dry conditions, Materials Today: Proceedings, 22 (2020) 726-736.
22. R. Gouveia, F. Silva, P. Reis, A. Baptista, Machining Duplex Stainless Steel: Comparative Study Regarding End Mill Coated Tools, Coatings, 6 (2016) 51.
23. L. Xian, H. Zhao, G. Xian, J. Xiong, H. Fan, H. Du, Effect of TiC addition and Co binder content in cemented carbide substrates on the microstructure and mechanical properties of the TiAlN-based composite films, Vacuum, 182 (2020) 109787.

24. G. Xian, J. Xiong, H. Zhao, H. Fan, Z. Li, H. Du, Evaluation of the structure and properties of the hard TiAlN-(TiAlN/CrAlSiN)-TiAlN multiple coatings deposited on different substrate materials, International Journal of Refractory Metals and Hard Materials, 85 (2019) 105056.
25. T. Sprute, W. Tillmann, D. Grisales, U. Selvadurai, G. Fischer, Influence of substrate pre-treatments on residual stresses and tribo-mechanical properties of TiAlN-based PVD coatings, Surface and Coatings Technology, 260 (2014) 369-379.
26. G. Skordaris, K.D. Bouzakis, T. Kotsanis, P. Charalampous, E. Bouzakis, B. Breidenstein, B. Bergmann, B. Denkena, Effect of PVD film's residual stresses on their mechanical properties, brittleness, adhesion and cutting performance of coated tools, CIRP Journal of Manufacturing Science and Technology, 18 (2017) 145-151.

Figures

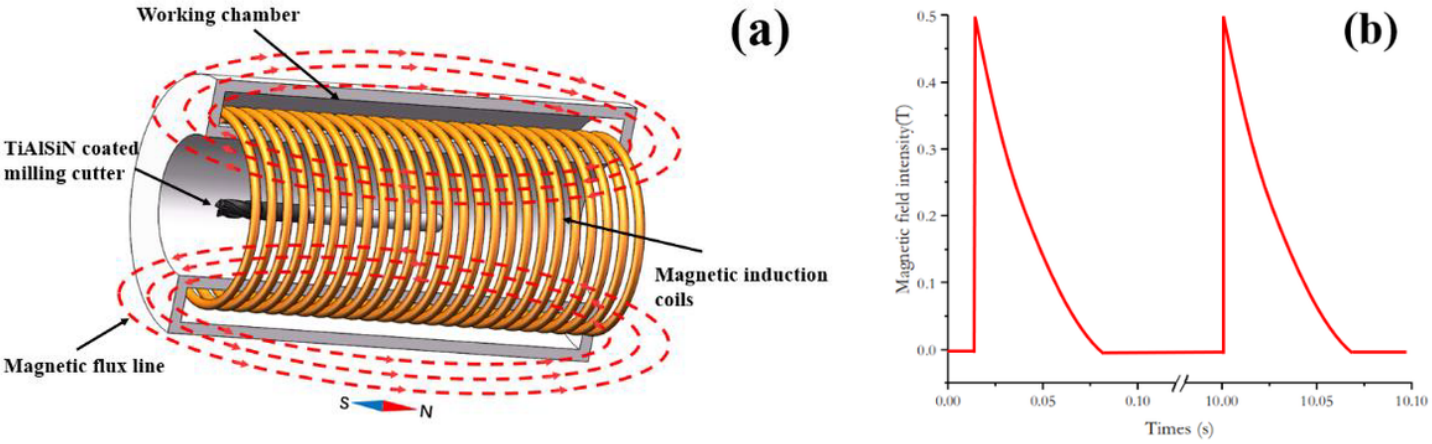

Figure 1

Schematic diagram of magnetic field treatment process (a) and the Variation of the pulsed magnetic field intensity (b)

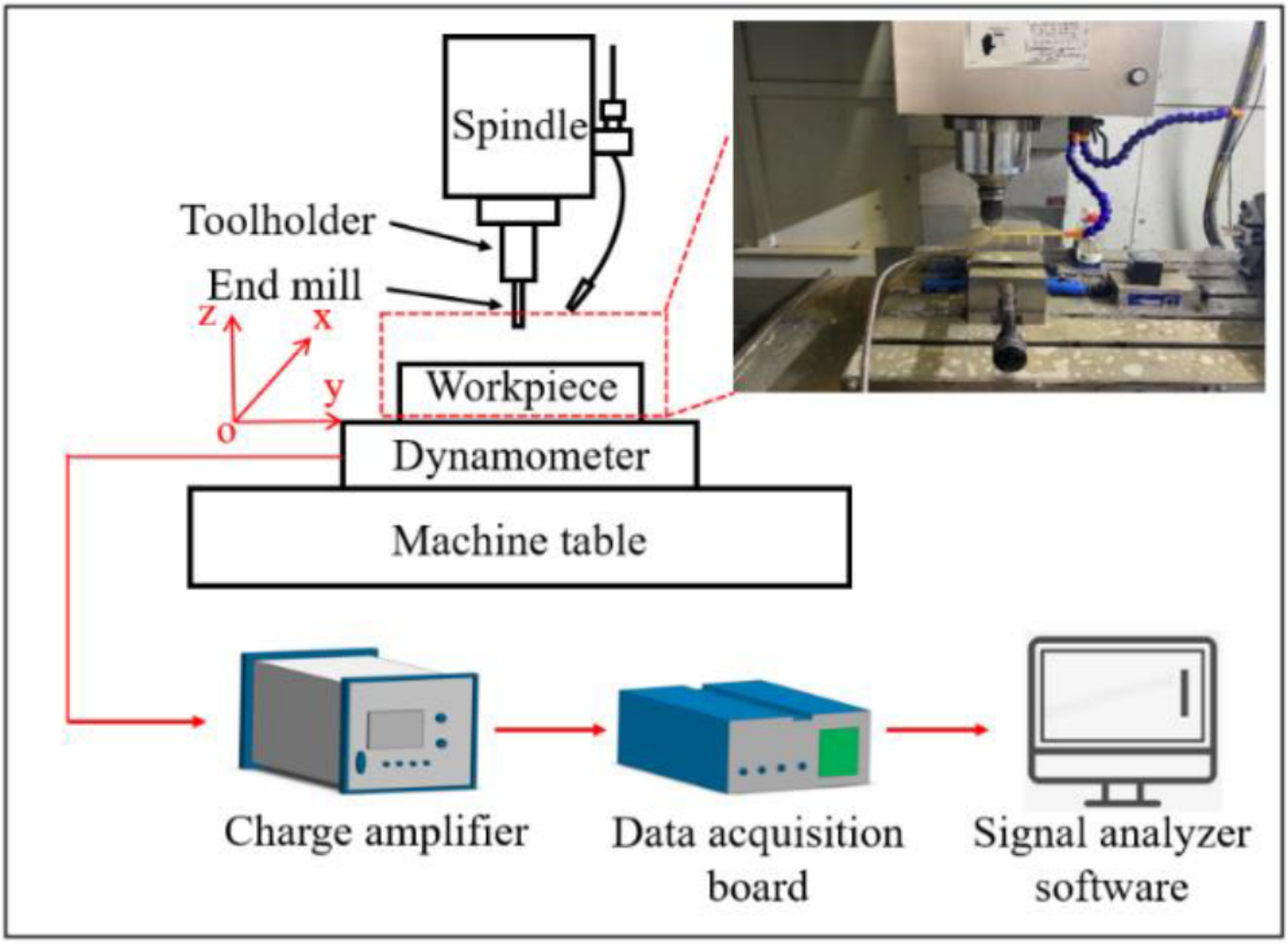

Figure 2

Illustration of the entire experimental process

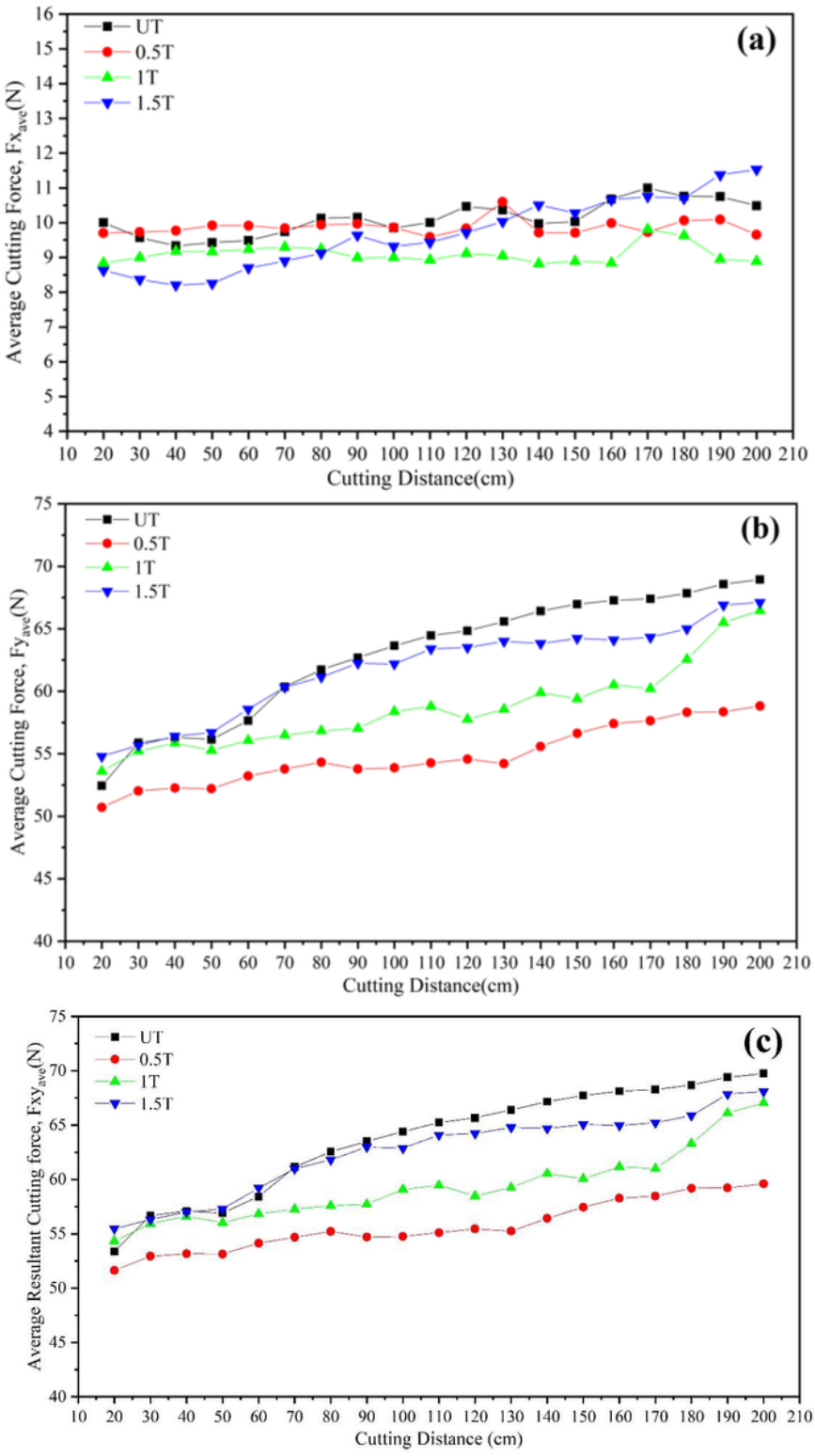

Figure 3

Variation of the cutting forces with cutting distance for the untreated tool and the tool treated by different magnetic field strength

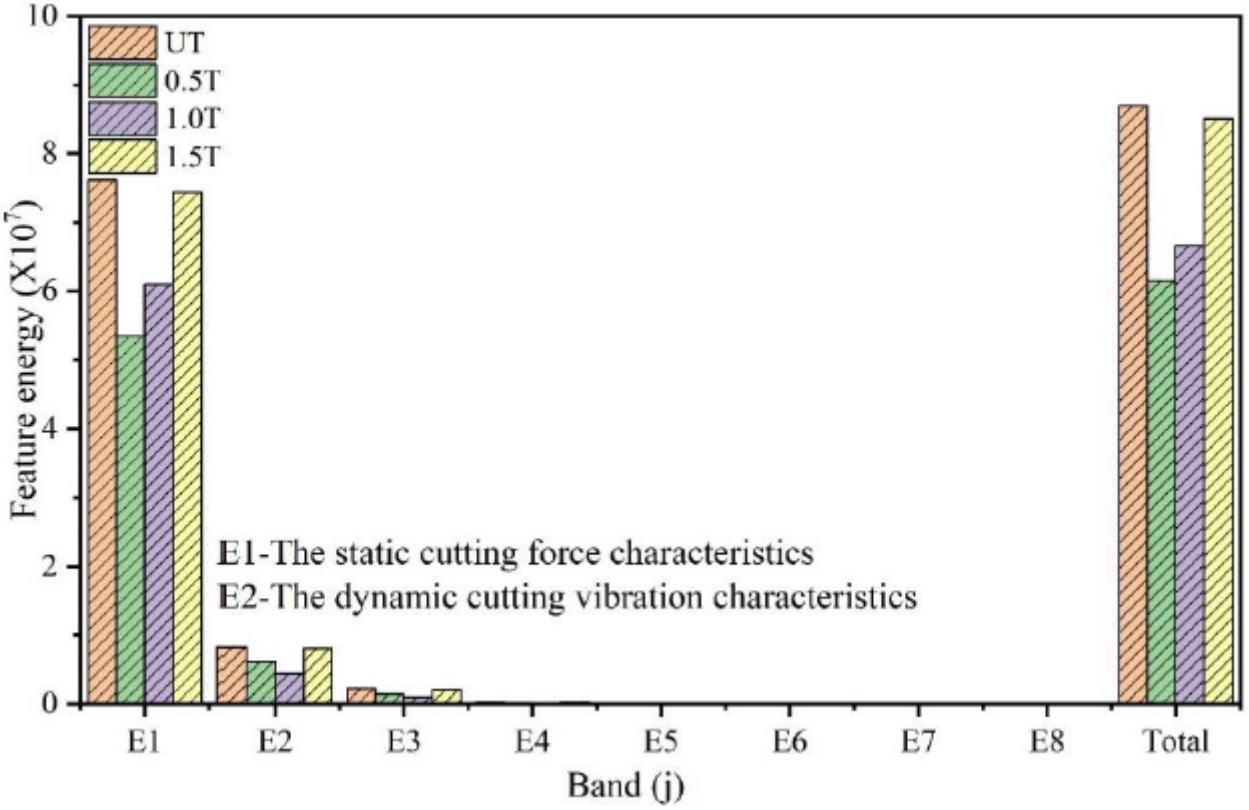

Figure 4

Comparison of the time-frequency domain feature energy of the m-th signal band and the total feature energy of all tools

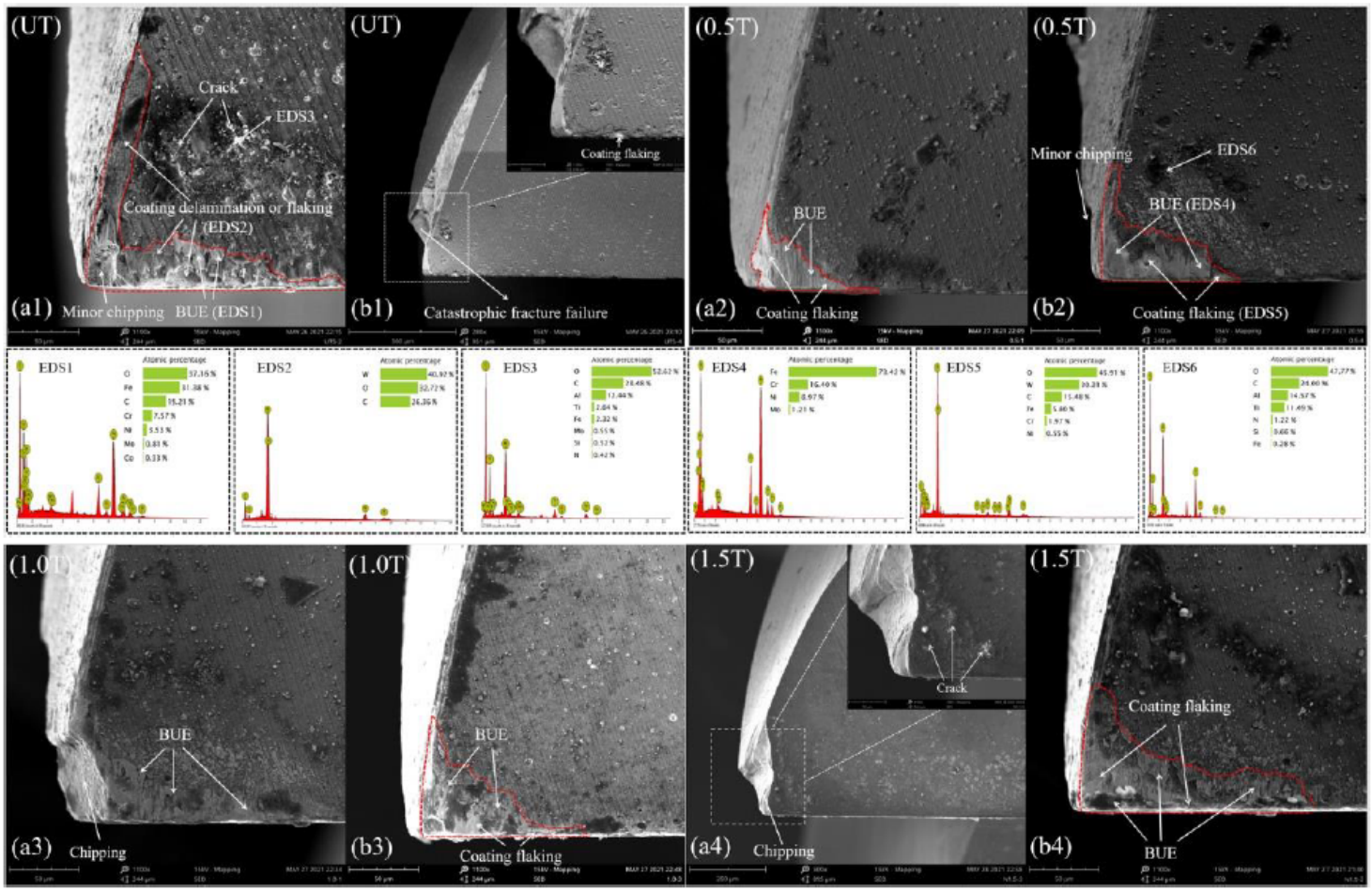

Figure 5

SEM images and EDS results of tool wear in the flank face. Long cutting edges(a1-a4); short cutting edges(b1-b4)

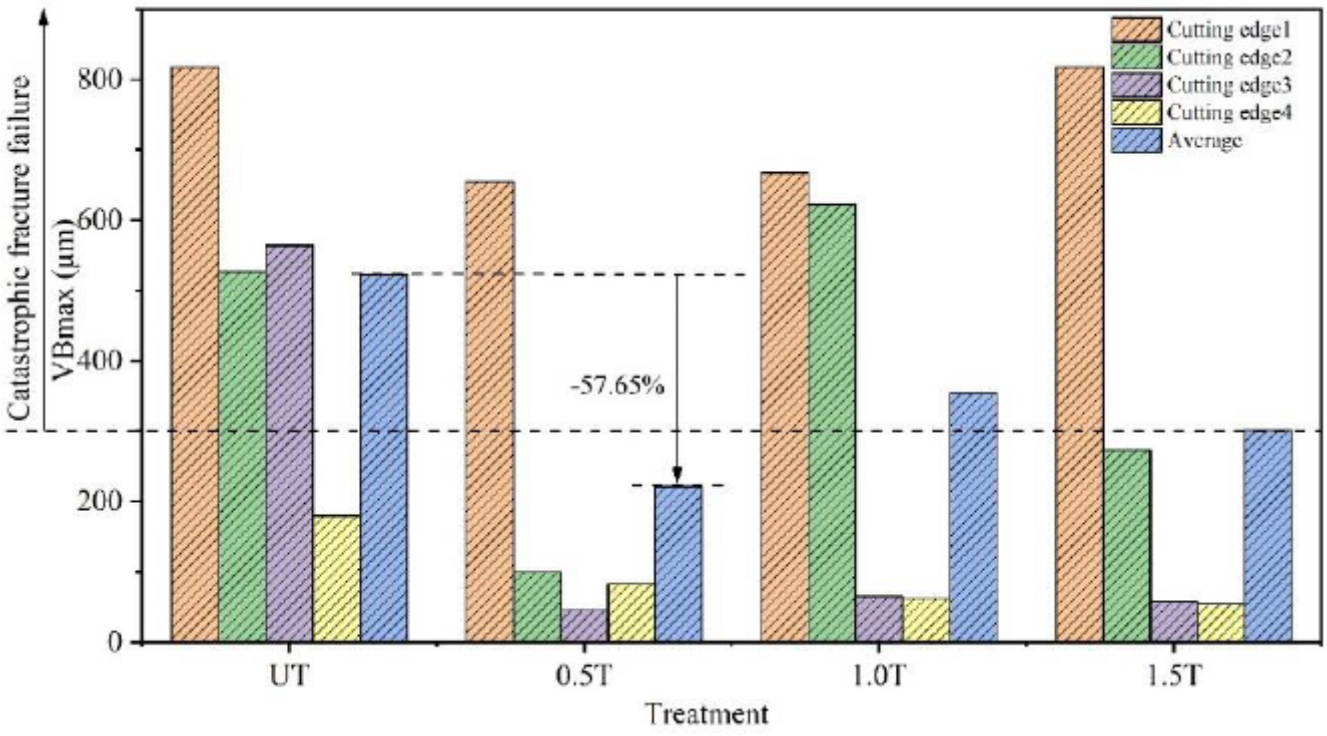

Figure 6

The wear widths of the flank face (VB_{max} and □ VB_{max}) after different treatment

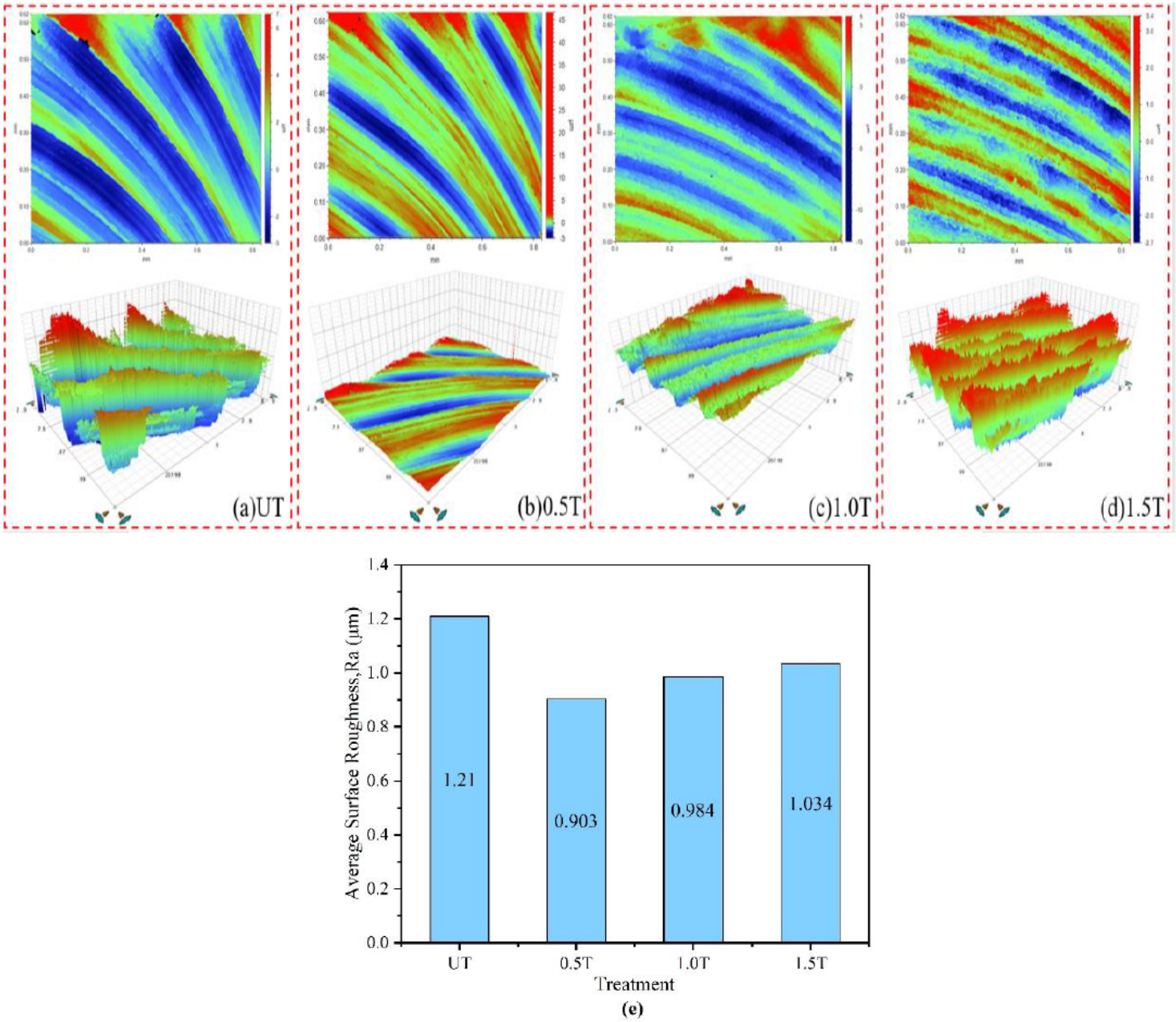

Figure 7

Surface profile (a-d) and average surface roughness (e) of the workpieces cut by tools treated by different fields

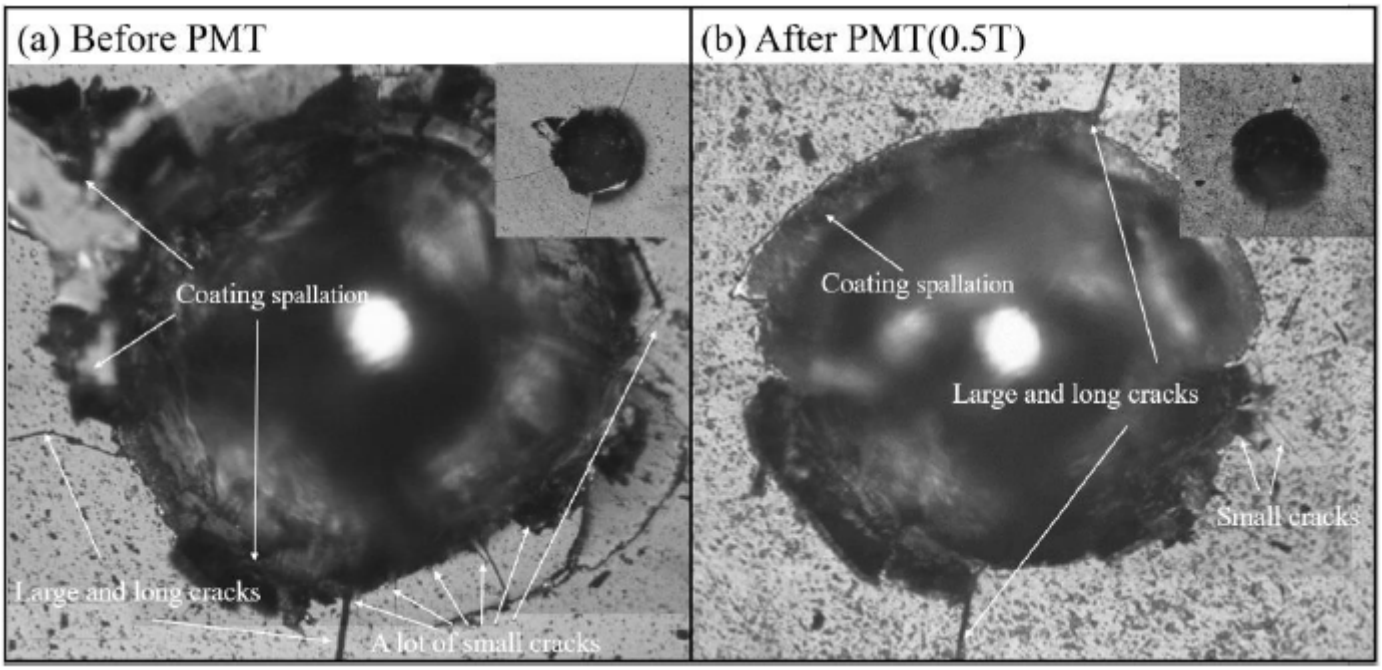

Figure 8

Indentations made with 60kg load in TiAlSiN coating deposited on WC-12wt%Co cemented carbide (a) Before PMT (b) After PMT (0.5T)

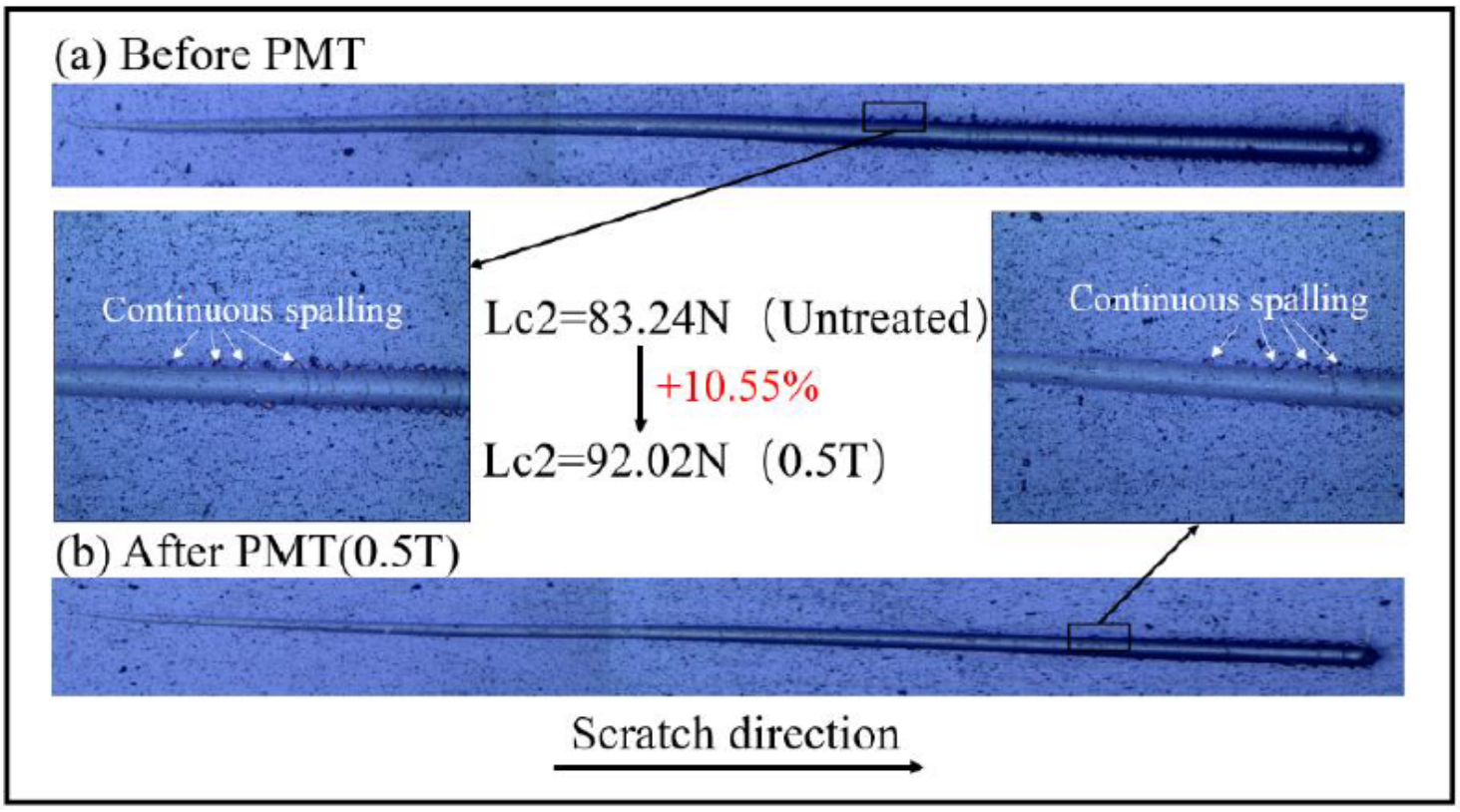

Figure 9

Scratch signals and adhesive failure morphologies of the TiAlSiN coating deposited on the WC-12wt%Co cemented carbide sample: (a) before PMT; (b) after PMT (0.5T)

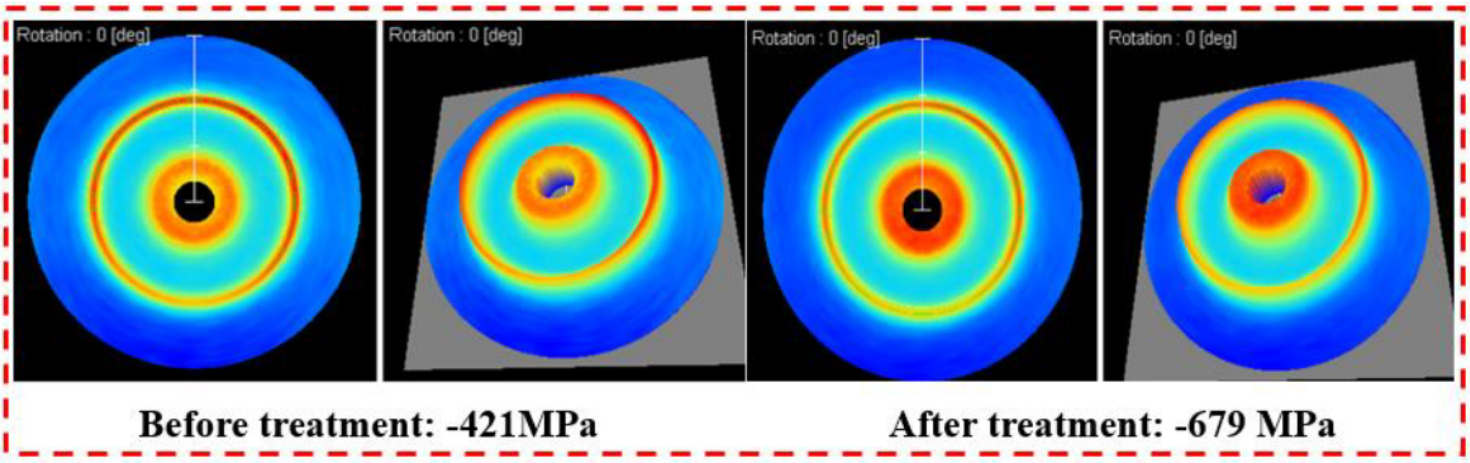

Figure 10

Residual stress in TiAlSiN coating before and after treatment (0.5T)

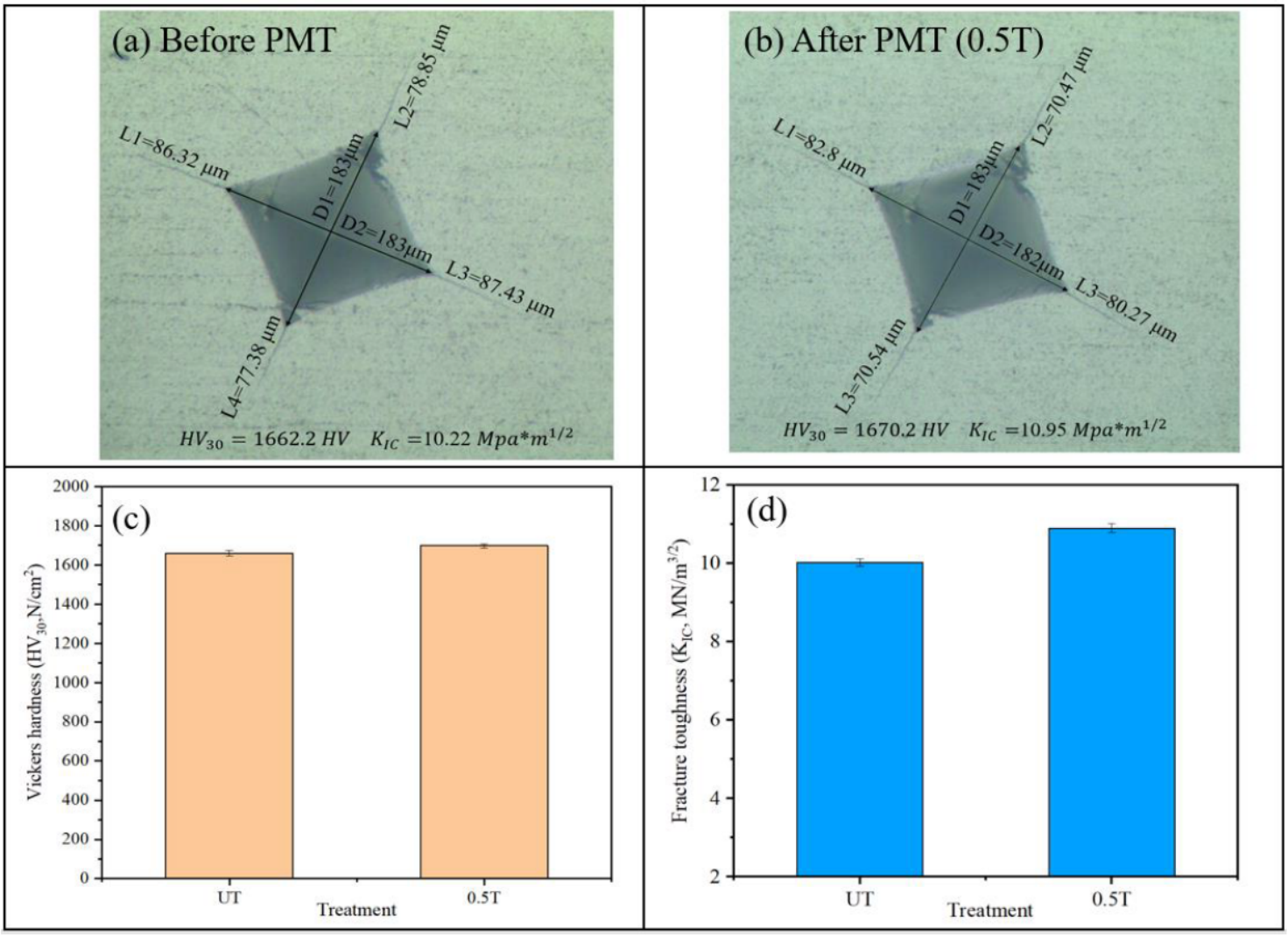

Figure 11

Vickers hardness and fracture toughness values of the untreated and 0.5 T treated WC-12wt%Co carbide cemented samples